Experimental Optics

Contact person:
Roland Ackermann
Friedrich-Schiller-Universität Jena
Abbe School of Photonics
Max-Wien-Platz 1
07743 Jena, Germany
Phone: +49 3641 9-47821, e-mail : Roland.Ackermann@uni-jena.de

Last edition: Roland Ackermann, February 2015

Lab Title: Adaptive Optics Laboratory Report

Group number	G 14
Student name(s)	Ke Li, Jerome Jahn
Name of TA	Kim Lammers
Date of Lab	March11,2019
Date of Final Report return	March14,2019

Adaptive Optics Laboratory Report

Ke Li, Jerome Jahn

March 2019

Contents

1 Introduction

In imaging system, different kinds of aberration are commonly expected due to both the influence of optical components and the environment. Although aberration from optical components could be carefully avoided by having good design of the components, in many imaging system, aberration caused by the environment are uncontrollable, thus it is necessary to have an alternative way to correct the aberration and improve the image qualities.[2]

Adaptive optics is one of the most important methods used to correct aberration of an imaging system. Using a Shack-Hartmann Wavefront Sensor(SHWS), and a deformable mirror, an adaptive optics system can algorithmically and dynamically correct different kinds of aberration, improving the image quality significantly.Thus, adaptive optics is widely used in various imaging systems.

In this laboratory, we used an adaptive optics system and conducted experiments to measure the waterfront of microscopic system and astronomic system and corrected the aberrations. We studied how to identify and correct different kinds of aberration and investigated the strength and limits of the adaptive optics system.

2 Theory

2.1 Shack-Hartmann Wavefront Sensor

In adaptive optics, a Shack-Hartmann wavefront sensor is normally used to detect and measure the deformation of the waves of the light source. A Shack-Hartmann wavefront sensor is composed of two parts, an array of lenses with the same focal length, and an array of photon sensor, usually a CCD sensor.

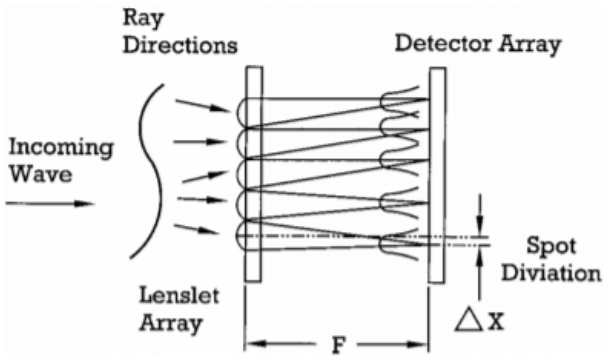

Figure 1: Shack-Hartmann Wavefront Sensor[1]

As shown in Figure 1, a deformation in the incoming wave will result in a deviation from the focal spot on the photon sensor. The deviation is labeled as

Spot Deviation Δx in the figure. The distance between the lenslet array and detector array is the focal length of the lenslet. The spot deviation Δx can determine the phase difference and the angle of the wavefront at each lenslet.

$$\theta = tan^{-1}(\frac{\Delta x}{F}) \tag{1}$$

where θ is the angel of the wavefront at the lenslet.

$$\Theta = k\frac{(\Delta x)^2}{2F} \tag{2}$$

where Θ is the phase difference.[1]

2.2 Aberration Theory using Zernike Polynomials

To understand the aberration of the imaging system, one normally analyze the wavefront of the light. Zernike Polynomials can be used to quantitatively analyze the aberration occurs in an imaging system based on the analysis of the wavefront. In many imaging systems, the aperture of is circular, requiring the polynomials to express aberration in the spherical coordinates. Zernike Polynomials express the any optical wavefront in a polynomial composed of the weight of different kinds of aberration terms:

$$W(r,\theta) = \sum_{n}^{k}\sum_{m=-n}^{n} W_n^m Z_n^m(r,\theta) \tag{3}$$

where r is the radial component of the function, θ is the azimuthal angel, W_n^m is the weighting coefficient, and Z_n^m is the Zernike polynomials, which can be expressed as:

$$Z_n^m(r,\theta) = \begin{cases} m > 0 : R_n^{-m}(r)\sin(-m\theta) \\ m \geq 0 : R_n^m(r)\cos(m\theta) \end{cases} \tag{4}$$

where R is the radial part of the polynomial, which could be expressed as:

$$R_n^m(r) = \sqrt{\frac{2(n+1)}{1+\delta_{m0}}}\sum_{s=0}^{\frac{n-m}{2}} \frac{(-1)^s(n-s)!}{s!\,(\frac{n+m}{2}-s)!\,(\frac{n-m}{2}-s)!} r^{n-2s} \tag{5}$$

The first 22 terms of the Zernike Polynomials and their corresponding aberration is shown in the figure below.

Index				
i	n	m	$Z_i(r, \theta)$	Aberration Term
1	0	0	1	Piston
2	1	1	$2r\cos(\theta)$	Tip
3	1	−1	$2r\sin(\theta)$	Tilt
4	2	0	$\sqrt{3}(2r^2 - 1)$	Defocus
5	2	2	$\sqrt{6}r^2\cos(2\theta)$	Astigmatism
6	2	−2	$\sqrt{6}r^2\sin(2\theta)$	Astigmatism
7	3	1	$2\sqrt{2}(3r^3 - 2r)\cos(\theta)$	Coma
8	3	−1	$2\sqrt{2}(3r^3 - 2r)\sin(\theta)$	Coma
9	3	3	$2\sqrt{2}r^3\cos(3\theta)$	
10	3	−3	$2\sqrt{2}r^3\sin(3\theta)$	
11	4	0	$\sqrt{5}(6r^4 - 6r^2 + 1)$	Spherical (1st)
12	4	2	$\sqrt{10}(4r^4 - 3r^2)\cos(2\theta)$	
13	4	−2	$\sqrt{10}(4r^4 - 3r^2)\sin(2\theta)$	
14	4	4	$\sqrt{10}r^4\cos(4\theta)$	
15	4	−4	$\sqrt{10}r^4\sin(4\theta)$	
16	5	1	$2\sqrt{3}(10r^5 - 12r^3 + 3r)\cos(\theta)$	
17	5	−1	$2\sqrt{3}(10r^5 - 12r^3 + 3r)\sin(\theta)$	
18	5	3	$2\sqrt{3}(5r^5 - 4r^3)\cos(3\theta)$	
19	5	−3	$2\sqrt{3}(5r^5 - 4r^3)\sin(3\theta)$	
20	5	5	$2\sqrt{3}r^5\cos(5\theta)$	
21	5	−5	$2\sqrt{3}r^5\sin(5\theta)$	
22	6	0	$\sqrt{7}(20r^6 - 30r^4 + 12r^2 - 1)$	Spherical (2nd)

Figure 2: First 22 Terms of the Zernike Polynomials[1]

2.3 Amplitude of the Defocus Term

Defocus is one of the most common optical aberrations occur when a focusing lens is used, and the image projected on the image plane is out of focus for environmental or internal optical system problems. The term in Zernike Polynomial that describes defocus is:

$$Z_0^2 = W_0^2\sqrt{3}(2\rho^2 - 1) \tag{6}$$

where W_0^2 is a scaling factor.

The wavefront coming out of a focusing lens to a focus point can be modeled as a spherical wave, whose radius of curvature could be expressed using Euclidean geometry.

$$\Delta = R - \sqrt{R^2 - a^2} \tag{7}$$

where R is the radius of curvature of the spherical wave, a is the size of the aperture of that the spherical wave enters, and Δ is the phase difference between the point at the center of the aperture to the edge of the aperture, as shown in Figure 3 below.

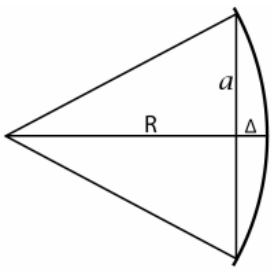

Figure 3: Spherical Wave with Radius of Curvature R Entering an Aperture with Size a[1]

Normalization of the Zernike polynomial gives us:

$$\Delta = \frac{a}{\lambda}(\sqrt{(\frac{R}{a})^2 - \rho^2} - \sqrt{(\frac{R}{a})^2 - (\frac{1}{\sqrt{2}})^2}) \tag{8}$$

Using Tyalor Expansion and further simplification of the equation gives us:

$$\Delta = -\frac{a^2}{4\sqrt{3}\lambda R}\sqrt{3}(2\rho^2 - 1) \tag{9}$$

from which we could derives the scaling factor of the defocus term:

$$W_2^0 = -\frac{a}{4\sqrt{3}\lambda R} \tag{10}$$

where a is the size of the aperture, λ is the wavelength of the light source, R is the radius of curvature of the spherical wave.

2.4 Deformable Mirror

Combining with a SHWS, a deformable mirror is used to adjust the distorted wavefront to eliminate the aberration of the optical system. Figure 4 is a structure of a typical deformable mirror. An optically flat membrane is suspended above a grid of electronic actuators. The d is the distance between the optical mirror membrance and the electronic actuators. For each electronic actuator, a high voltage can be supplied to it, resulting in a strong attracting force from the actuator to mirror membrane at specific location. When the voltage difference is applied programmatically according to the needs of adjustment of a wavefront, different optical aberration can be corrected.

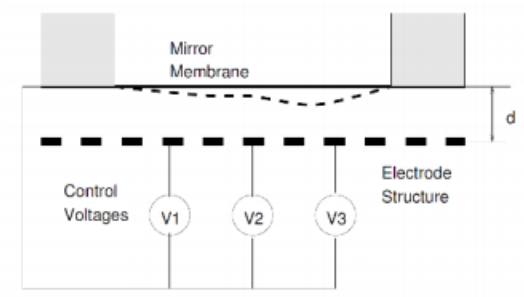

Figure 4: Deformable Mirror[1]

2.5 Wavefront Aberration Function

The wavefront surface calculated by the Frontsurfer software calculates the wavefront surface in terms of a deviation from an ideal plane wave. The parameters listed to describe this surface include the Peak-to-Valley distance, the RMS wavefront error, and the Strehl Ratio.

These parameters are based on analyzing the phase difference of the actual wavefront to the reference wavefront at each point in the plane transverse to the optical axis. This phase difference is expressed in units of full wave cycles, or waves. The Peak-to-Valley aberration value specifies the maximum difference between points on the measured wavefront in units of waves. The RMS wavefront error is a measure of the average difference in phase between the wavefront and the reference wavefront over the entire wavefront (2). The Strehl ratio is the ratio of the peak image intensity of the aberrated wave to the peak intensity of the unaberrated wave. The Strehl ratio is thus a measure of the degree to which the aberrations affect the system. The higher the Strehl ratio, the less effect the aberrations have on aspects of the image such as the contrast. The lower the Strehl ratio, the more these aberrations dominate the actual intensity pattern at the image plane.

3 Experimental Procedures

3.1 Alignment of the Shack-Hartmann wavefront sensor

Before beginning the measurement, we first aligned the adaptive optics system in use. We centered the position of the SHWS so that all lenslets are illuminated , and the illumination area was at the center of the CCD images captured on the computer screen. We aligned the laser beam so that the beam passed through the central position for each optical components in used in the system. To find the optimal exposure , we captured and analyzed images using different filters, and recorded the optimal filter when the images of the SHWS captured by the

CCD camera is either over-exposed or under-exposed.

3.2 Wavefront analysis with a Shack-Hartmann wavefront sensor

After properly aligned and calibrate the wavefront sensor, in the second part of the experiment, we analyzed the wavefront with SHWS and the algorithm provided on a third party software with the setup shown in figure below:

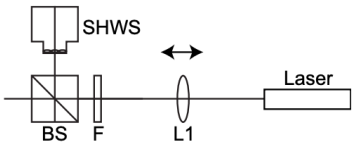

Figure 5: Wavefront Analysis Experiment Setup[1]

In the figure, SHWS is the Shack-Hartmann wavefront sensor, BS is a beam spilter, F is the optical filter wheel, L1 is the focus lens for the laser to obtain a spherical wavefront. [1] We applied filter 2 of on the filter wheel to avoid the problems caused by over-exposure of the laser on the sensor, and obtained the aberration analysis results from the program of the inteferogram and different Zernike Polynomials terms for 10 positions between the filter wheel and the laser. We recorded the distances and the amplitude of the defocus term to further analyze the maximum tilt angle and radius of curvature of the wavefront.

3.3 Aberration compensation in a microscope using a deformable mirror

In this part of the experiment, we analyzed the aberration compensation in a microscope using a deformable mirror. The experimental setup is shown in Figure 6 below.

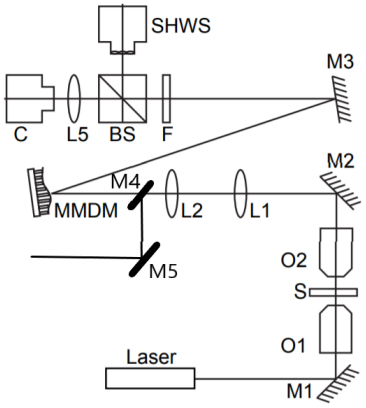

Figure 6: Experimental setup for aberration compensation in a microscope using a deformable mirror[1]

Light is emitted by a laser and reflected off of mirror M1. It passes through a microscope objective O1 that focuses the beam onto a platform for placing samples in the path of the light. Microscope objective O2 collimates the beam again. The beam reflects off of mirror M2 and is led along a horizontal stretch that includes lens mounts L1 and L2 and an insertable mirror M4. This optional mirror would intercept that leads the light the beam is collim reflects off of mirror M2.

After properly align the system, we calibrate the system by setting all values of the attenuator to zero, and select the optimal filter to obtain good quality images of the SHWS. We inserted microscope lens under the microscope, analyzed and compensanted the aberration caused by the microscope slide with the software and the deformable mirror. In this experiment, we also investigated the maximum number of slides under the microscope we could insert so that the adaptive optics system can still adjust the aberration causes by the deformable mirror.

3.4 Optimization of a telescope using wavefront analysis

In this part of the experiment, we used the adaptive optics system to examine the alignment of a telescope system we built, and correct the aberration with the help of the closed loop method in the Frontsurfer software. The experimental setup is shown in the figure below.

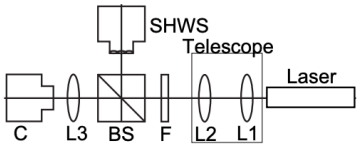

Figure 7: Experimental setup for telescope optimization analysis[1]

4 Results

4.1 Alignment of the Shack-Hartmann wavefront sensor

Before beginning measuring the wavefront of an optical system, we first aligned the SHWS to an optimal position, and find the optimal filter to avoid over-exposure and under-exposure effect of the SHWS images. In the figure below, image (a) is the image of SHWS observed by the CCD camera when no filter was applied. An effect of over exposure was observed. In image (b), filter 2 was applied, reducing the intensity of the light, thus, the over-exposure effect was reduced, in image (c), filter 5 was applied, causing under-exposure effect so that image of SHWS is no longer visible.

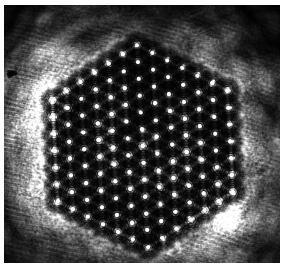

(a) Without Filter SHWS Image

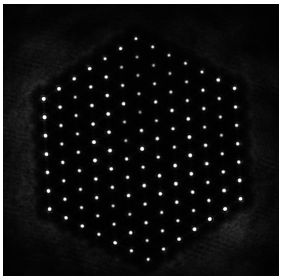

(b) Second Filter, SHWS Image

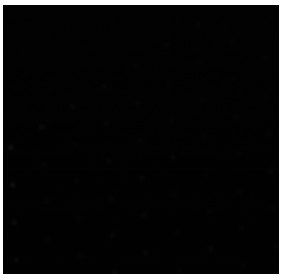

(c) Fifth Filter, SHWS Image

Each filter also produced a wavefront surface, which was a visual representation of the wavefront aberration function. The results for all six filters are shown in Figure 9

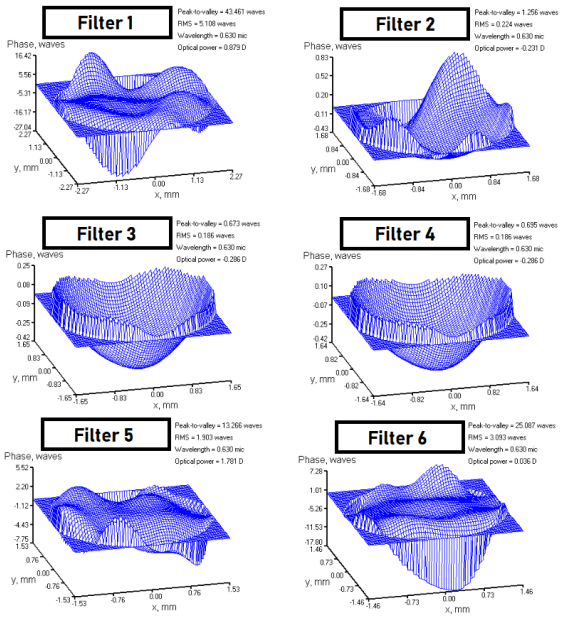

Figure 9: Wavefront Surfaces Generated After Light Transmission through Filters 1-6

4.2 Wavefront analysis with a Shack-Hartmann wavefront sensor

It was planned to perform measurements of the wavefront at 10 different positions of the lens. In total, nine positions of the lens were measured for their wavefront output. The tenth run did not save properly. The lens was moved from a separation of 1.5 cm from the mount to 9.5 cm separation from the mount in 8 consecutive 1 cm steps. At each step, the intensity on the camera was analyzed, and the coefficients of the Zernike polynomials was computed. The uncertainty in the position of the lens on the optical axis was determined to be plus or minus 1 millimeter, as a handheld ruler was used in order to read off the position. Incorrect positioning of the ruler or shaky hands could have compromised the measurement.

The distance from the SHWS to the beam splitter was measured to be 16.2 $\pm$ 0.2 cm. The distance from the beam splitter to the starting position of the left edge of the lens mount was measured as 5.2 $\pm$ 0.2 cm. The distance from the left edge of the lens mount to the center of the lens was measured to be 2.3 $\pm$.05 cm. The uncertainty in the absolute position of the left edge of the lens mount at each position is determined to be 0.1 cm. These uncertainties stem from measuring the distances with a handheld ruler. Incorrect positioning or shaky hands could have resulted in a displacement of the measured value from the true value by the uncertainty bounds given above.

The interferograms at the measured positions are shown in the figure below. The interferograms are shown in Figure 10.

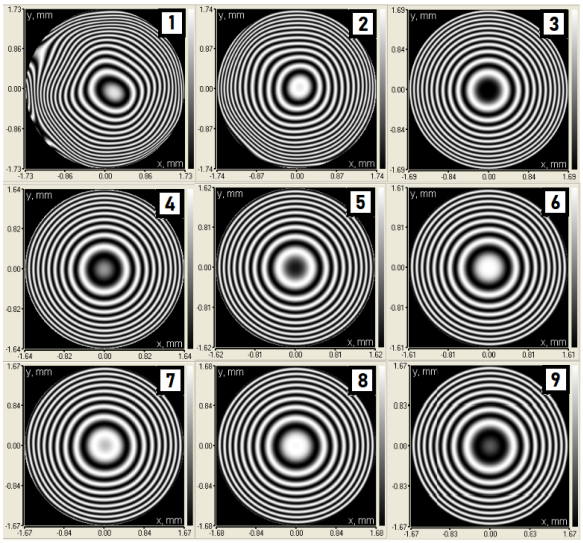

Figure 10: Interferogram of the lens positions 1-9

The interferograms where the lens is closer to the SHWS show more aberrations than when the lens is further away from the SHWS. The lens position values are reported in terms of distance of the center of the lens to the SHWS. The results for the resulting amplitude of the defocus term are written in Table 1.

Distance (cm)	Unc. (cm)	Defocus Amplitude (unitless)	Unc. (unitless)
23.7	0.55	8.607937	5E-07
24.7	0.55	7.299405	5E-07
25.7	0.55	7.658553	5E-07
26.7	0.55	6.848538	5E-07
27.7	0.55	6.467924	5E-07
28.7	0.55	6.089023	5E-07
29.7	0.55	6.222807	5E-07
30.7	0.55	6.167736	5E-07
31.7	0.55	6.807072	5E-07

Table 1: Measured Lens Distance from SHWS against Amplitude of Defocus in Measured Wavefront

The values in the above table are plotted in the figure below.

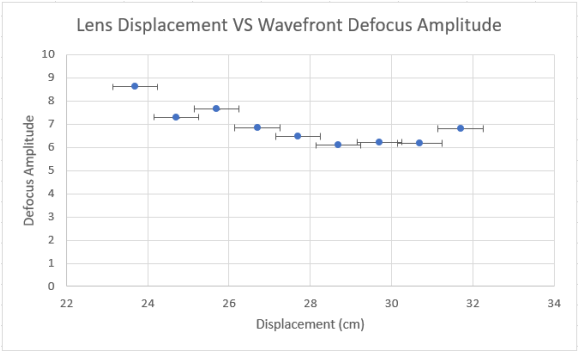

Figure 11: Lens Displacement from Original Position Plotted Against Amplitude of Defocus in Wavefront Measured by SHWS

There is a downward trend when looking at the data as a whole. The measured data cannot be called linear, as the uncertainty in the defocus amplitude is so small.

The minimum radius of curvature measured in this experiment can be calculated from the equation below

$$W_2^0 = -\frac{a^2}{4\sqrt{3}\lambda R}, \tag{11}$$

where the left side is the defocus amplitude, a is the distance from the center of the beam to the edge, λ is the wavelength the program used to calculate the interferogram given as 630 nm, and R is the radius of curvature of the wavefront incident on the SHWS. The size of the beam a corresponds to the distance from the center of the interferogram to the edge. The table below shows the values of a, the amplitude, and the calculated radius of curvature.

Defocus Amplitude	a (mm)	Unc (mm)	Radius of Curvature (mm)	Unc. (mm)
8.607937	1.73	0.005	-80.9	0.23
7.299405	1.74	0.005	-96.5	0.28
7.658553	1.69	0.005	-86.8	0.26
6.848538	1.64	0.005	-91.4	0.28
6.467924	1.62	0.005	-94.4	0.29
6.089023	1.61	0.005	-99.1	0.31
6.222807	1.67	0.005	-104.3	0.31
6.167736	1.68	0.005	-106.5	0.32
6.807072	1.67	0.005	-95.3	0.29

Table 2: Calculation of the Radii of Curvature of the Wavefronts incident on the SHWS at each Position

The uncertainty in the value was calculated by considering the relative uncertainties of the quantities used to calculate it. As the quantities used were

provided by the software, the highest relative uncertainty was in the value of a, stemming from the program providing only three significant digits. This was the predominant source of uncertainty. The minimum radius of curvature measured was then -80.9 ± .23 mm.

From the radius of curvature, the maximum measured tilt can be found. The following equation stemming from chord length is used:

$$\sin\theta/2 = \frac{a}{R}, \tag{12}$$

where θ is the wavefront tilt. This maximum is thus found as

$$\theta = 2\arcsin\frac{1.73}{-80.9} = .042 radians. \tag{13}$$

The next largest aberration measured was the spherical aberration of the wavefront. The values of the spherical aberration are shown in Table 3 below.

Distance (cm)	Unc. (cm)	Sph. Aberration Amplitude (unitless)	Unc. (unitless)
23.7	0.55	-0.1631739	5E-08
24.7	0.55	-1.169612	5E-07
25.7	0.55	0.1688155	5E-08
26.7	0.55	0.1051550	5E-08
27.7	0.55	0.1037465	5E-08
28.7	0.55	0.09750979	5E-09
29.7	0.55	.06105201	5E-09
30.7	0.55	0.1757494	5E-08
31.7	0.55	0.1379009	5E-08

Table 3: Measured Lens Distance from SHWS against Amplitude of Spherical Aberration in Measured Wavefront

The uncertainty in the amplitudes of Tables1 and 3 is from the reporting error of the software, which simply did not report more than 6 digits. There was no estimate of the uncertainty of the amplitude besides this choice in reporting the number of digits.

The data in Table 3 is plotted in the figure below.

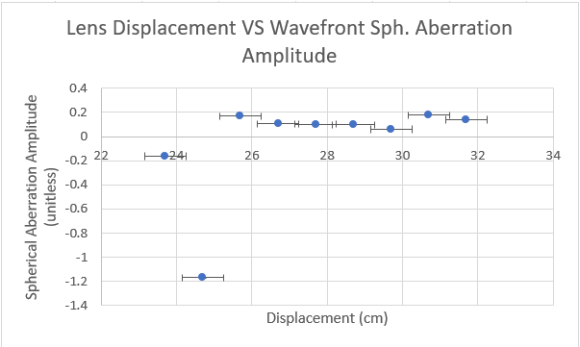

Figure 12: Lens Displacement from Original Position Plotted Against Amplitude of Spherical Aberration in Wavefront Measured by SHWS

The data did not follow any functional trend. The magnitude of the amplitudes of spherical aberration are about one order of magnitude less than the amplitude of the defocus aberration.

The Strehl ratio at the first 7 positions was 0.000, while it rose to 0.001 for the last two data points. This was a highly suspicious result, as it implies that there was no peak intensity at all in the image plane for the first 7 positions. This is impossible however, as there were measured interferograms in Figure 10. Thus, it was concluded that the intensity must have been so small compared to the expected value that the Frontrunner software rounded the value down to 0.000.

4.3 Aberration compensation in a microscope using a deformable mirror

The interferograms for each trial are shown in Figure 13.

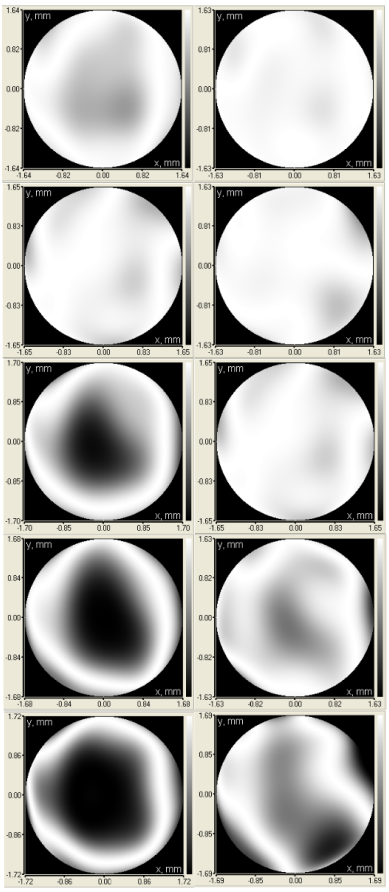

Figure 13: Interferogram of the Different Combinations of Slides. Left column is slides 1-5 Without MMDM Correction, Right column is Slides 1-5 With MMDM Correction

The row number in the above picture is equal to the number of slides. The first column represents the aberrated wavefront, the second column represents the MMDM corrected wavefront. As can be seen, the larger the aberration, the less the deformable mirror is able to correct the aberration.

As we can see from the inteferogram, the adaptive system reached it's limit for compensating for the aberration caused by the microscope slides when the number of slides reached to 5.

The Wavefront surfaces for each slide are shown in Figure 14

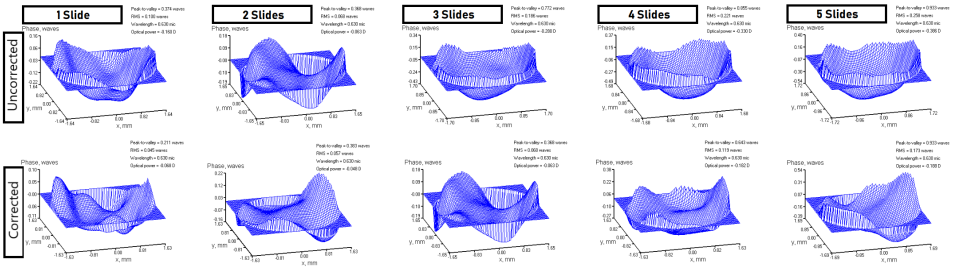

Figure 14: Wavefront Surface Measured by SHWS for Different Amounts of Slides.

From the aberration report and our theoretical prediction, the largest source of aberration of this experiment is defocus. The values of the defocus term and the Strehl ratio before and after the compensation is shown in the table below:

S	Defocus(WO, waves)	Strehl (WO)	Defocus (W,Waves)	Strehl(W)
1	0.235 ± 0.01	0.729	0.0901 ± 0.01	0.939
2	missing	missing	0.0696 ± 0.01	0.872
3	0.447 ± 0.01	0.339	0.0947 ± 0.01	0.823
4	0.511 ± 0.01	0.159	0.266 ± 0.01	0.659
5	0.625 ± 0.01	0.109	0.2947 ± 0.01	0.337

Table 4: Result of defocus term and the Strehl ratio before and after the compensation. S stands for the number of sildes. WO means the defocus and Strehl term measured without compensation, W means the quantities measured with compensation. The uncertainties came from the misalignment of the system.

As we can observe from the data in the table, as the number of slides increases, the Strehl value decreases, and the number of waves in the defocus term increases. Such general trend is valid based on the theory that the increase in the number of slides will block more light, reducing the Strehl intensity, and increasing the defocus of the microscope. As we can also see from the table when comparing to the defocus term before and after the compensation that as the number of slides increase, the ability of the deformable mirror to correct the aberration is less. When the number of slides reached 5, defocus is still a significant part of the aberration.

To further examine the relation between number of microscope slides and the Strehl ratio and defocus term, we plotted the measurement data and performed a linear fit to the data points, as shown in the figure below:

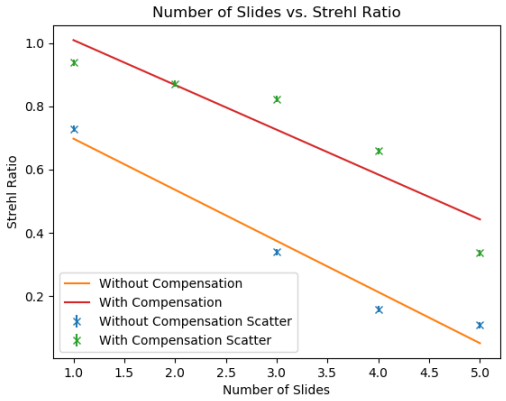

Figure 15: Linear fit and scatter plot of number of microscope slides and the Strehl ratio.

The slope of the linear fit without compensation is: -0.617 ± 0.0074, the intercept is: 0.859 ± 0.026, the R value is: 0.982. The slope of the linear fit with compensation is: -0.142 ± 0.007, the intercept is: 1.1510.038, the R value is: 0.93. As the R values of the linear fit show, the number of slides and the Strehl ratio show confirms to a linear relation over 90% of time, which matches our expectation of the behavior of the SHWS. The errors of the measurement and linear fit result might come from the misalignment of the system.

It is also noticeable from our aberration report that sometime astigmatism is the major source of the aberration, after the wavefront adjustment of the deformable mirror. This also could be explained theoretically that after adjustment, when defocus is no longer the most significant source of aberration of the system, the aberration was dominated by the astigmatism caused by the deformable mirror having different radii of curvature in different radial directions.

4.4 Optimization of a telescope using wavefront analysis

In this part of the experiment, we could examine the quality of the alignment of our telescope using the aberration evaluation function of the adaptive optics system. After carefully aligned the optical system, the result of the wavefront measurement is shown in the figure below:

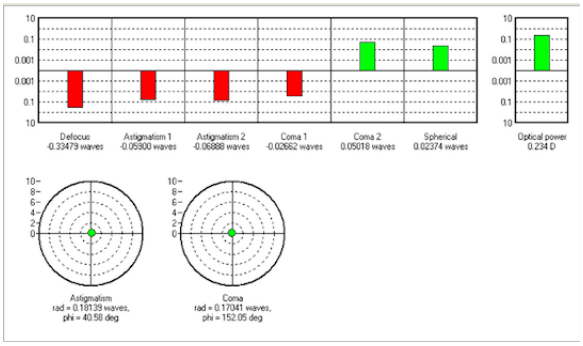

Figure 16: Telescope Alignment Examination Result

As we can see from the evaluation result, defocus is still a dominate source of aberration of our optical system. We then used the micrometer screw to realign the telescope, and applied the loop function of Frontsurfer to eliminate the defocus aberration of the telescope system. The examination result after adjustment of the alignment is shown in the figure below.

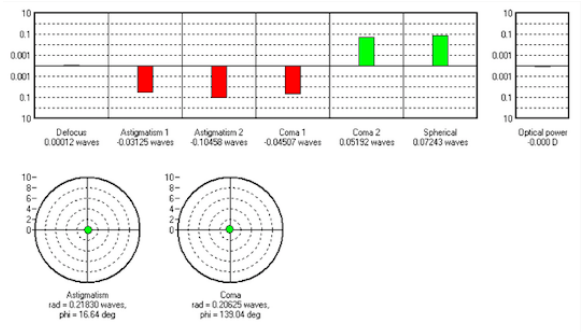

Figure 17: Examination Result after Adjustment of the Alignment

As we can see from the figure above, adptive optics system has the powerful function to reduce small aberration in a telescope system even down to zero.

5 Discussion

5.1 Wavefront Aberrations from a Lens

The amplitudes of the two most prominent wavefront aberrations were found to change with the position of the lens. Increasing the distance that the SHWS was to the lens, and thereby increasing the distance between the SHWS and the lens' focal plane, resulted in a generally decreasing defocus amplitude, which leveled out and then increased again. Concluding a linear relationship between

these variables from our data would be erroneous. The expected result for this relationship is that a change in the distance, unless the beam is moving through the defocus, should result in a uni-directional movement of the amplitude of the defocus term. The defocus should get a larger amplitude the further away the measurement plane is from the focal plane. The observed data does not follow this simple relationship. Instead, this pattern seems to fit the situation of moving the focal plane from behind the SHWS to in front of the SHWS. The defocus then reached a minimum value right when the SHWS was moving through the depth of focus. This is what was observed. The focal length of the lens used would need to be determined to compare this result to the truly expected result given the distance values used.

The minimum measured radius of curvature was -80.9 $\pm$ .47 mm. This was much smaller than the calculated theoretical value of 457 mm. The theoretical did not lie within the bounds set by the uncertainty. There was an alarmingly high percent error of 82%. The maximum wavefront tilt was found to be .042 $\pm$ .00024 radians. This was smaller than the maximum wavefront tilt measurable, which was .457 radians.

The reason for the radius of curvature that was measured being smaller than the calculated theoretical value most likely stems from the determination of the size of the beam. The experimental size of the interferogram that was used as the aperture size a in the equation is not the same thing as the aperture of the SHWS being 1.9 mm. In fact, the smaller value used to calculate this, namely 1.73, is a source of error. If 1.9 mm had been used to calculate the beam radius, a value of -97.6 $\pm$ .56 mm results. This is closer to the theoretical minimum. Further

If a more accurate value was used in the theoretical calculation that corresponds more with the type of calculation used for the experimental value, the comparison of the two may yield a more insightful conclusion.

The spherical aberration amplitude generally increased with the movement of the lens, although there were plenty of exceptions. The expected result was that the spherical aberration should not be a function of the distance of the lens from the SHWS, as the spherical aberration is something imbued in the wavefront after exiting the lens. Propagation through space should not change the amount of spherical aberration present in the measured wavefront. The result then may indicate more about the type of analysis done by the software on the measured points.

The Strehl ratio was extremely low for all of these measurements. More information about specifically how the program used calculates the Strehl ratio would be useful in evaluation the source of this perplexing result.

There is the possibility of a systematic error, although the SHWS was calibrated nicely and the alignment of the laser beam through the mirrors was also verified. The systematic error would then have to do with the interaction of the setup with the software. The SHWS points rarely were all recognized by the software. This could be improved through the use of filters better suited for the goal. During the experiment, there was not much choice between filters. Having more nuanced filters, or perhaps a filter able to dynamically change the trans-

mission in order to optimize the intensity of the light incident on the SHWS, would improve measurements and provide clues as to what to investigate further in order to ascertain the roots of the observed aberration patterns.

5.2 Correcting Aberrations from Slide in Microscope

The MMDM was able to improve the aberrations in all cases. The worse the aberration, the worse the corrected wavefront was as well. This was most likely due to the deformable mirror having a maximum possible deformation. In future experiments, a deformable mirror that can attain a smaller radius of curvature than the one used in this experiment could be used. As the MMDM to a certain extent improved the aberrations of all of the slides, it is difficult to say how many slides it can handle. Our measurement stops at the fifth slide, due to our observation from the inteferogram and the aberration report that the defocus aberration is still the dominating aberration term even after the correction of MMDM.

The trend of the Strehl ratio follows our expectation, although the trend is not perfectly linear as predicted by the theory, we obtained reasonable measurement considering the errors caused by possible misalignment of the setup. In the future experiment to study the aberration compensation in a microscope, we could take more data points, increases the quality of the lens and the alignment to improve the accuracy of the measurement.

We could also use a filter that dynamically adjusts its transmission to maximize the intensity of light hitting the SHWS. This would increase the data points that the software uses to calculate the amplitudes of the Zernike Polynoms.

6 Conclusion

In this set of experiments, the optical aberration of defocus as well as the operation and capabilities of a closed-loop adaptive optics system were tested. The system consisted of a Shack-Hartmann Wavefront Sensor (SHWS) and a Deformable Mirror (MMDM) It was found that the amplitude of the defocus Zernike polynom changed in proportion to the distance of the focal plane of the lens from the SHWS. The spherical aberration was relatively unaffected by the movement. The deformable mirror was able to correct the aberration of microscope lens up to 4 to 5 microscope slides. It was also tested that adaptive optics is useful in testing the quality of the alignment of a telescope. For small aberration, the closed loop function was able to reduce the defocus aberration of the telescope down to zero. Future experiments would benefit from having a more specialized filter for optimizing the light intensity incident on the SHWS. This would maximize the points that the software utilizes, and it would be an easy additional functionality of the software in calibrating itself. In essence, the filter would be adjusted through a range of values and returned to the value that yielded the maximum number of light points that the software registers and is

able to use. Apart from that, having the software calculate its own uncertainty in the amplitudes of the Zernike Polynoms would make the results more reliable.

7 Preliminary and Final Questions

7.1 Preliminary Questions

- The microlens array used, has 127 microlenses. They have a pitch of 300 m and a focal length of 18 mm. Compute the maximal wavefront tilt θ that is measurable without focusing into the square of the adjacent microlens. The illuminating laser has a wavelength of $\lambda = 632nm$. To what phase difference Θ does the wavefront tilt correspond?

  According to equation 1) in the theory section, the maximal wavefront tilt could be calculated from (1)

  where Δx is the transversal displacement of the focal position from the focal point of a wavefront perpendicular to the optical axis, and F is the focal length. The pitch in this case corresponds to the side length of one square element in the array of lenslets, and so if one focal position were to move half that distance, the Δx would correspond to 150 microns. Then, the angle is calculated as:

  $$\theta = \arctan(.15/18) = 8.3 \times 10^{-3} = 0.4758^{\circ}, \tag{14}$$

  where the answer is in radians.

  This corresponds to a phase difference calculated using (15). The answer is then calculated as:

  $$\Theta = \frac{2\pi(.15)^2}{2 * 18 * .000632} = 6.21, \tag{15}$$

  where the answer is also in radians.

- Estimate the minimum wavefront tilt that is measurable. The pixel size of the CCD is $9.9 \times 9.9\mu m^2$

  The CCD can register two different tilt positions if a focal spot moves from one of its cells to the next. This is the minimum movement necessary to be able to distinguish the two signals. Thus, to find the minimum wavefront tilt, Equation (1) is used again. The assumption is made that a point of focused light starts out in the center of one CCD pixel, and needs to move to the other in order to have its movement be detected. Thus, the Δx is half of one pixel length, making it 4.5 microns. The minimum wavefront tilt is then calculated as:

  $$\theta = \arctan(.045/18) = 2.5 * 10^{-3}, \tag{16}$$

  where the answer is in radians.

- The hexagonal microlens array has an average aperture radius of a = 1.9 mm. Given the maximal wavefront tilt angle θ from the first question, what is the minimal curvature radius the SHWS is able to measure?

  The minimal curvature radius would be formed when the outermost lenses in the hexagonal array are measuring the maximum wavefront tilt. The following equation involving the chord length of a circle is used:

$$\sin \theta/2 = \frac{a}{R}, \tag{17}$$

  where a is the distance from the center of the hexagonal array to one of the vertices, θ is the maximum wavefront tilt, and R is the radius of curvature of the wavefront. The distance a is given as 1.9 mm. Then, the minimal curvature radius is computed as:

$$R = \frac{1.9}{\sin 8.3 * 10^{-3}/2} = 457, \tag{18}$$

  where the answer is in mm.

- The MMDM has an aperture of 2a = 15 mm, the maximal deformation the central attenuator can achieve is d = 9.5 μm. If used as a spherical mirror, what is the minimal focal length f that can be achieved?

  For a spherical mirror, the radius of curvature R is related to the focal length F through the expression:

$$F = \frac{R}{2}. \tag{19}$$

  The minimal focal length thus corresponds to the minimal radius of curvature of the mirror. The following equation involving the chord of a circle will be used in order to find the radius of curvature R:

$$\Delta = R - \sqrt{R^2 - a^2}, \tag{20}$$

  where a is half of the chord length and Δ is the distance from the center-point of the chord to the edge of the circle. In this case, Δ is given as 9.5 microns and a is given as 7.5 mm. R is then calculated as:

$$.0095 = R - \sqrt{R^2 - (7.5)^2}, R = 2961, \tag{21}$$

  where the answer is in mm. The minimal focal length is then solved for as

$$F = 1.48, \tag{22}$$

  where the answer is in meters.

- How are the Zernike-Polynoms defined? Which aberration do they describe?

  The Zernike-Polynoms are a complete set of orthogonal functions that are able to be summed up to generate any wavefront surface. Each Polynom corresponds to a particular aberration. All aberrations can be described as a Zernike-Polynom. Defocus, spherical aberration, astigmatism, and coma are just a few examples. The coefficients in the function decomposition into Zernike-Polynoms describe the relative amounts of each aberration present in the wavefront which is their sum.

7.2 Final Questions

- For which beams SHWS and MMDM work best and why?

  The SHWS and MMDM work best for beams with radius of curvature greater than 6 meters. This is because the SHWS can only register radii of curvature above this value, whereas the MMDM is capable of outputting radii of curvature that are smaller.

  They also work best for beams that have a beam waist much smaller than the MMDM and that fully illuminate SHWS. This is a range of beam waists for which the minimum is set by the SHWS and the maximum by the MMDM.

- How do specific aberrations affect the image quality / resolution / point spread function?

  The aberrations in general decrease the image quality by decreasing the Strehl ratio. Thus, the original image becomes more blurred and the peak intensity decreases. This decreases the resolution from the optimal aberration-free diffraction-limited resolution. The point spread function at the image plane becomes a blurred version of what it would be in the diffraction-limited case.

- Which are the predominant aberrations and how can they best be compensated for? Which aberrations should be better compensated within the static setup?

  The predominant aberrations are defocus and spherical aberration. The defocus can be compensated for by either fixing the source of the aberration by properly focusing the light onto the image plane or by using a MMDM to correct the aberrated wavefront. Spherical abberation can be compensated by using different optical components or by using a MMDM. Within a static setup, the aberrations that can be better compensated are defocus, as the position of the objects within the static setup determines the amplitude of defocus. The other aberrations have more to do with the quality of the optical components used.

- Where are the limits of dynamic wavefront correction? The limits of dynamic wavefront correction are set by the maximum deformation of

the MMDM. They are also set by the speed at which aberrations are changing, as it takes time to send information to the mirror and have it readjust. The reaction time of the mirror needs to be less than the period between changes in the wavefront aberrations for example. This becomes important when attempting to use dynamic wavefront correction in very dynamic systems, such as astronomical data-taking for light coming through a turbulent atmosphere or the light source being a very dynamic system such as plasma.

8 References

[1] Ulrike Blumroeder. *Adaptive Optics*. Abbe School of Photonics. March 2013

[2] J.C. Wyant, Katherine Creath. *Basic Wavefront Aberration Theory for Optical Metrology*. Applied Optics and Optical Engineering, Vol. XI. Academic Press, Inc. 1992.

[3] *Introduction to Adaptive Optics and Deformable Mirrors*, Edmund Optics. `https://www.edmundoptics.com/resources/application-notes/optics/introduction-to-adaptive-optics-and-deformable-mirrors/`